Thermal Science and Engineering Progress 9 (2019) 169–176

Contents lists available at ScienceDirect

Thermal Science and Engineering Progress

journal homepage: www.elsevier.com/locate/tsep

Applications and perspectives of gas analysis based on sonar instrumentation

C. Rossi[a,*], M. Battistin[b], C. Bortolin[b], O. Crespo-Lopez[b], C. Deterre[c], M. Doubek[d], G. Hallewell[e], S. Katunin[f], K. Nagai[g], B. Pearson[h], D. Robinson[i], A. Rozanov[e], V. Vacek[d], L. Zwalinski[b]

[a] INFN Genova, via Dodecaneso 33, 16146 Genova, Italy
[b] CERN, 1211 Geneva 23, Switzerland
[c] DESY, Notkestraße 85, Hamburg 22607, Germany
[d] Czech Technical University, Technická 4, 166 07 Prague 6, Czech Republic
[e] Aix Marseille Université, CNRS/IN2P3, CPPM, Marseille, France
[f] B.P. Konstantinov PNPI, 188300 St. Petersburg, Russia
[g] Dept. of Physics, Oxford University, Keble Road, Oxford OX1 3RH, UK
[h] Max-Planck-Institut für Physik, Föhringer Ring 6, 80805 München, Germany
[i] Dept. of Physics, Cambridge University, J. J. Thomson Avenue, Cambridge CB3 0HE, UK

ARTICLE INFO

Keywords:
Evaporative cooling
Heat transfer coefficient
Ultrasonic
Zeotropic blends
Thermosiphon
Gas analysis

ABSTRACT

We have developed ultrasonic instrumentation to simultaneously monitor flow and composition in a variety of gas mixtures. Flow and mixture composition are respectively derived from measurements of the difference and average of sound transit times in two opposite directions in a flowing process gas blend. Gas composition is then determined from an automated comparison of the measured sound velocities with a velocity/composition database.

Continuous, real-time precision measurements of binary gas mixtures are required in many applications. While the most natural application of this instrumentation is in the analysis of such mixtures, analysis of mixtures with additional components is also possible, as discussed in this paper.

In the ATLAS experiment at CERN, several instruments are presently used in the Detector Control System. Three instruments monitor octafluoropropane (C_3F_8, R218) and carbon dioxide (CO_2, R744) coolant leaks into the nitrogen-purged envelopes surrounding elements of the inner silicon tracker. Precision in molar concentration of better than 2.10^{-5} is routinely seen in mixtures of C_3F_8 in nitrogen in the presence of known concentrations of the third party gas CO_2.

Two further instruments are used to monitor the new 60 kW thermosiphon C_3F_8 evaporative coolant recirculator which exploits the 90 m depth of the ATLAS pit to circulate coolant without the need for pumps or compressors in the primary loop. These instruments are used to verify the absence of air leaks in the thermosiphon cooling circuit and to measure the vapour-phase coolant flow in real-time.

This instrumentation is also used to measure zeotropic fluorocarbon blends containing C_3F_8 and up to 25% hexafluoroethane (C_2F_6, R116), achieving a precision around 0.16% in the range 0–25% C_2F_6. We also report on measurements of heat transfer coefficient in these blends: our experimental data were compared to several empirical correlations, with typical differences less than 10%.

This analysis technique, targeting binary pairs of gases of dissimilar molecular weight, is particularly promising for mixtures of anesthetic gases, including in the developing area of anesthesia using xenon. The instrument and its various applications will be discussed.

1. Introduction

The ultrasonic instrumentation is based on the measurement of sound transit times in opposite directions in a flowing process gas to determine its characteristics in real time. Measurements are made using pairs of 50 kHz bi-directional ultrasonic transducers [1] placed within flanged envelopes through which different mixtures flow. Synchronous with the emission of an ultrasound pulse a transit time clock is started.

* Corresponding author.
E-mail address: cecilia.rossi@cern.ch (C. Rossi).

https://doi.org/10.1016/j.tsep.2018.10.015
Received 8 April 2018; Received in revised form 4 October 2018; Accepted 29 October 2018

The clock is stopped by an above-threshold signal at the receiving transducer. Sound velocity is deduced from the average of the pairs of bi-directional transit times and is used to evaluate the concentration of the two principal components in a gas blend through real-time comparison of measured sound velocity with a stored *concentration vs. sound velocity* database, which takes into account the measured process temperature and pressure, as well as the known concentrations of background contaminant gases. The instrumentation exploits the physical phenomenon whereby – at known temperature and pressure – the sound velocity depends on the molar concentrations of its components and the known concentrations of third-party gases. The related database can be generated from theoretical models and/or from previously-made calibration mixtures [2,3].

Simultaneously in the same instrument the flow rate can be computed from the difference in transit times in the opposite directions and the geometrical parameters of the tube.

2. Principle of operation

The gas analysis algorithm is based on the general equation for sound velocity, c, in a gas:

$$c = \sqrt{\frac{\gamma RT}{M}} \tag{1}$$

where R is the molar gas constant (8.314 J·mol^{-1}·K^{-1}) and T is the absolute temperature in degrees Kelvin. The adiabatic index γ for the mixture is given by the ratio of the weighted sums of molar specific heat at constant pressure (C_{p_i}) to that at constant volume (C_{v_i}) of the n components:

$$\gamma_m = \frac{C_{pm}}{C_{vm}} = \frac{\sum_i w_i C_{p_i}}{\sum_i w_i C_{v_i}} \tag{2}$$

where w_i are the molar fractions of the components ($i = 1 \rightarrow n$). Similarly, the molar mass of the mix in kg·mol^{-1} is given by the weighed sum of the molar masses of each component, M_i

$$M = \sum_i w_i M_i \tag{3}$$

In this way Eq. (1) becomes:

$$c = \sqrt{\frac{\frac{\sum_i w_i Cp_i}{\sum_i w_i Cv_i} RT}{\sum_i w_i M_i}} \tag{4}$$

Fig. 1 illustrates as an example the variation of sound velocity with the concentration of C_3F_8 in N_2 (m.w. = 28) in the range 0 → 1%; a gas pair of interest in the ATLAS inner tracker cooling application. The added horizontal and vertical indicators illustrate the relationship between the uncertainties in measured sound velocity, ∂c, and mixture determination, $\partial(mix)$. At any concentration of the two components;

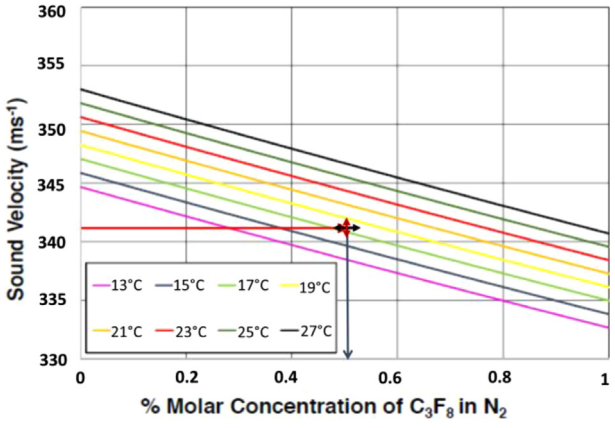

Fig. 1. Variation of sound velocity with concentration of binary C_3F_8/N_2 mixtures in the range 0 → 1% C_3F_8. The added indices illustrate the relation between the uncertainties in measured sound velocity and mixture determination [3].

$$\partial(mix) = \frac{\partial c}{m} \tag{5}$$

where m is the local slope of the *sound velocity vs. concentration* curve.

For each pair of gases of primary interest a (*sound velocity, concentration*) database is generated, covering the expected ranges of the primary gas mixture, process temperature and pressure and (where present) independently-measured concentrations of known third-party gases. The *sound velocity, concentration* data is stored as a series of polynomial fit parameters calculated at grid values of temperature, pressure and third-party gas concentration. In this regard, the effect on the mixture sound velocity of third-party gases can be calculated using Eq. (4) with the C_{p_i} and C_{v_i}data for the individual gas components derived from equations of state: for example in [4].

Our instruments give a typical sound velocity measurement error of better than ± 0.025 ms^{-1}, due to the following contributing uncertainties:

- ± 0.1 °C in gas temperature (± 0.02 ms^{-1});
- ± 1 mbar in gas pressure (± 0.003 ms^{-1});
- ± 0.1 mm in transducer spacing, based on prior calibration in at least two pure gases [5] (± 0.002 ms^{-1});
- ± 25 ns transit clock frequency (± 0.002 ms^{-1});

In the example from Fig. 1 the average slope of the *sound velocity vs. molar concentration* curve is around −12.25 ms^{-1} per percent of C_3F_8 in the range of interest of 0–1% molar C_3F_8. The ± 0.025 ms^{-1} instrument uncertainty in sound velocity results in a corresponding mixture uncertainty of ± 2.10^{-5}.

3. Applications of the instrument

Five ultrasonic instruments are currently integrated into the ATLAS DCS (*Detector Control System*) [3]. In the present implementation gas mixture analysis and flow are calculated in scripts running under Siemens SIMATIC WinCC v3.1.5 on Linux in a DELL Poweredge R610 SCADA (*Supervisory, Control & Data Acquisition*) computer. In future implementations this analysis could be carried out in firmware embedded in the microcontrollers of individual instruments.

Most of the instruments are used in the analysis of gas blends containing octafluoropropane (R218: C_3F_8), a fluid chosen for its non-flammability, dielectric and radiation-resistant properties. Zeotropic blends with up to 25% hexafluoroethane (R116: C_2F_6) are being considered as a means of reducing the operating temperature (and retarding the radiation damage) of the ATLAS silicon tracker. These blends have been set up with the aid of ultrasonic gas analysis, their evaluation is discussed in Section 4.

3.1. Real-time monitoring of the ATLAS C_3F_8 thermosiphon cooling circulator

Two ultrasonic instruments (also simply referred to as 'sonars') are used in the primary coolant loop of the new C_3F_8 ATLAS 60 kW thermosiphon (TS) evaporative coolant recirculator (Fig. 2) [5,6] at the CERN LHC (Large Hadron Collider).

This external plant exploits the (~90 m) height difference between the ground surface and the ATLAS underground experimental cavern to drive the natural circulation of the coolant, avoiding any active components in the C_3F_8 primary coolant circuit.

One instrument is configured as an angled flowmeter [2,7] and used to measure C_3F_8 vapor return mass flow (up to 1.2 kg·s^{-1}) to the condenser. A second instrument monitors air ingress to the condenser – the

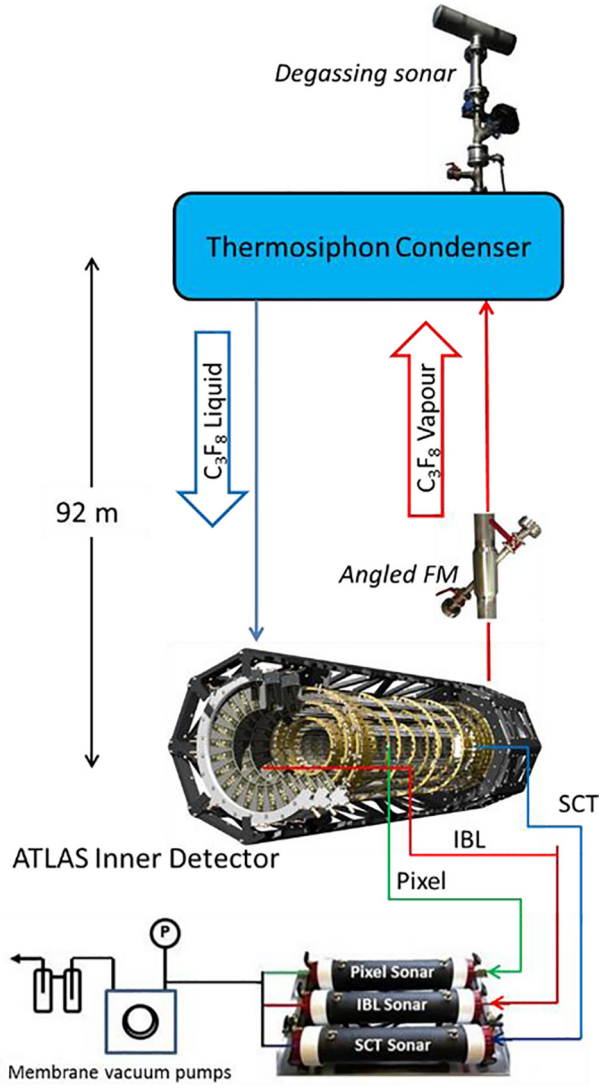

Fig. 2. Positions of the five ultrasonic instruments installed as part of the detector control system of the ATLAS tracking detector.

lowest pressure and highest part of the circulator allowing accumulated air to be "degassed".

Both instruments are located on the low pressure side of the cycle, as highlighted in the thermodynamic cycle in Fig. 3:

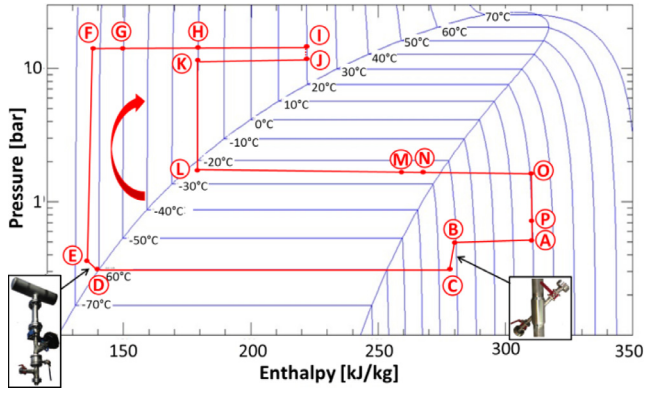

Fig. 3. Positions of the ultrasonic vapor flowmeter and condenser "degassing" instruments in the context of the C_3F_8 thermodynamic cycle in the ATLAS 60 kW TS coolant recirculation plant.

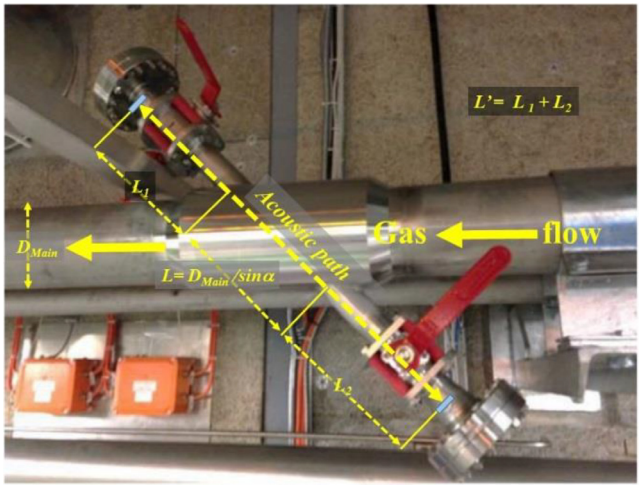

Fig. 4. The angled ultrasonic flowmeter installed in the ATLAS thermosiphon vapor return line.

- The vapor flowmeter in the ATLAS experimental cavern at the base of the superheated vapor column returning to the condenser;
- The "degassing" sonar at the headspace of the condenser on the surface.

3.1.1. *The angled ultrasonic flowmeter*

In the vapor flowmeter illustrated in Fig. 4 the ultrasound transit times t_{up}, t_{down}, are measured in opposite directions at 45° to the direction of gas flowing in a 131 mm diameter main tube. The acoustic path is composed of component lengths;

- $D_{Main}/\sin\alpha$, ($\alpha = 45°$); where the gas is in laminar motion in the main tube of internal diameter D_{Main};
- L'; where the gas is considered static in the acoustic side-arms.
- The flow velocity, $\boldsymbol{v}$ (ms^{-1}), is expressed as:

$$v = \frac{c\left(ct_{up} - \frac{D_{Main}}{\sin\alpha} - L^{'}\right)}{\cos\alpha\,(ct_{up} - L^{'})}$$

$$\text{or} v = \frac{c\left(\frac{D_{Main}}{\sin\alpha} + L^{'} - ct_{down}\right)}{\cos\alpha\,(ct_{down} - L^{'})} \quad (6)$$

with volumetric flow obtained by multiplying v by the cross sectional area of the main tube.

The ultrasonic transducers were positioned in side arms to minimize pressure drop and turbulence in the main tube. Quarter-turn ball valves with 40 mm diameter orifices allow the sound to pass but can be closed for transducer access without interrupting the C_3F_8 vapor flow or exposing it to air pollution. A pressure transducer and three thermistors monitor each side arm to allow the density of the circulating C_3F_8 vapor to be calculated for logging mass flow. Multiple thermistors are installed for redundancy. The average of the three readings in each side arm is logged, with the on-line algorithm configured to reject any sensor whose value deviates from the average of the three by more than a specified amount. The flowmeter demonstrated linearity in air flows up to 10 ms^{-1} (131 $l{\cdot}s^{-1}$) before installation, with an *rms* precision of ± 2.3% of full scale [7].

Fig. 5 illustrates flowmeter measurements in C_3F_8 vapor during commissioning tests of the ATLAS TS in April 2017.

During these commissioning tests the ATLAS SCT and Pixel sub-detectors were evaporatively cooled with C_3F_8 at power levels of 20 kW. With only the ATLAS "barrel SCT" sub-detector powered (a) the dissipation of nearly 22 kW required the circulation of around 0.4 $kg{\cdot}s^{-1}$ of C_3F_8. The corresponding mass flow with the full SCT

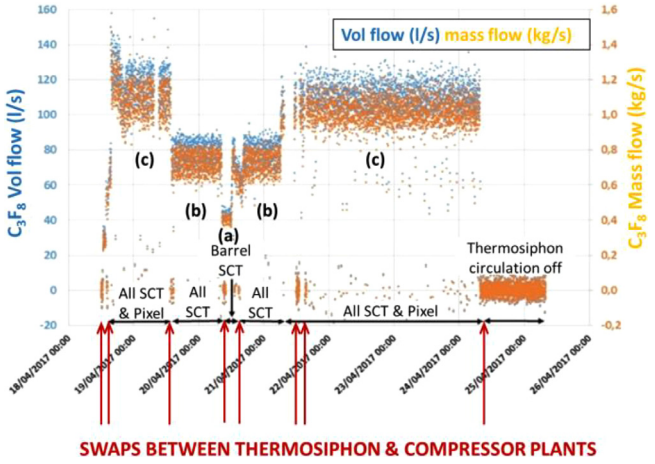

Fig. 5. C_3F_8 volumetric and mass flow measured in the angled ultrasonic flowmeter in the ATLAS TS vapor return line (April 2017) under different load conditions (a), (b) (c): see text.

("barrel" and "endcaps") powered (b) was around 0.75 $kg{\cdot}s^{-1}$, while that required to cool the combined SCT and Pixel trackers (c) was around 1.1 $kg{\cdot}s^{-1}$, as illustrated in Fig. 5. The mass flow resolution of the ultrasonic flowmeter during these runs was around ± 0.05 $kg{\cdot}s^{-1}$.

During the commissioning tests repeated transitions (cold "swaps": red arrows in Fig. 5) were made between the TS and the compressor-driven recirculator that it will replace. During these swaps the temperature fluctuations on powered silicon modules were less than 2 °C. Note: during compressor operation zero flow is seen in the C_3F_8 vapor return line to the condenser since the vapor is redirected to the compressor inputs.

3.1.2. *The "degassing" sonar*

The "degassing" sonar (illustrated in Figs. 2 and 6) detects and eliminates ingressed air from the TS plant. It is mounted on the top of the TS condenser, at the highest point (also the lowest temperature and pressure region of the TS) where ingressed air would tend to accumulate.

The accumulation of ingressed air must be avoided since an increase in effective condenser pressure will erode the pressure differential needed to return the 1.1 $kg{\cdot}s^{-1}$ C_3F_8 vapor flow to the condenser against gravity.

The degassing sonar monitors the concentration of air through changes in sound transit time for a given temperature and pressure. In order to correctly measure the temperature of the gas, the sonar tube is

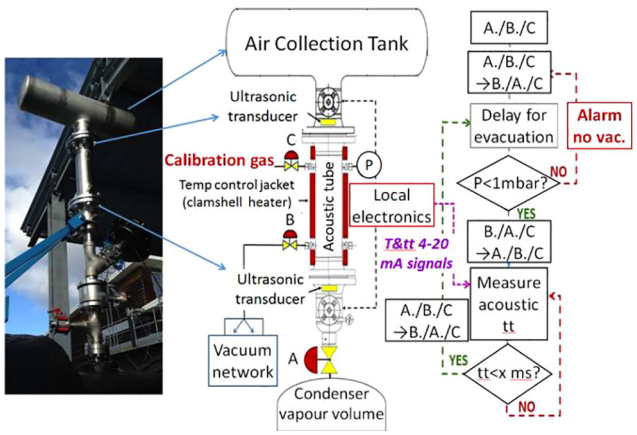

Fig. 6. *Left:* The degassing sonar installed on the thermosiphon condenser; *right:* the automatic response matrix for valve control to vent air accumulated in the degassing sonar, based on sound transit time.

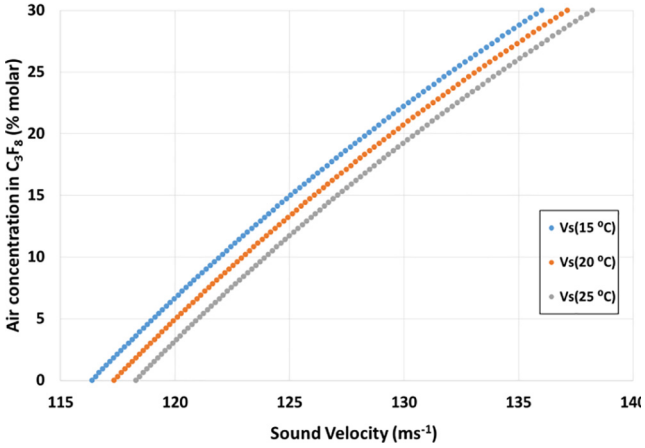

Fig. 7. Sound velocity dependence on air concentration in C_3F_8 vapor at three temperatures of the degassing sonar and a pressure of 300 $mbar_{abs}$.

protected by an external heating jacket. Due to their molecular weight (m.w.) difference (m.w. air = 29; m.w. C_3F_8 = 188), air will tend to accumulate in the collection tank above the instrument, decreasing the transit time over the acoustic path. When this falls below an operator-definable threshold known to be equivalent to a certain air concentration, the sonar tube and collection tank are isolated from the condenser vapor volume and evacuated to "release" the incondensable air.

Fig. 7 illustrates the variation of concentration of air in C_3F_8 *vs* measured sound velocity at three different temperatures for a pressure of 300 $mbar_{abs}$.

The large dynamic range of interest for air infiltration into C_3F_8 requires quadratic (3-parameter) fits of *concentration vs. sound velocity*. These are based on 100 points (in 0.3% increments of concentration) generated in a temperature-pressure grid from 10 to 45 °C (step 1 °C: n_T = 41 points) and 300–1500 $mbar_{abs}$ (step 100 mbar: n_P = 13 points), resulting in 1599 stored parameters ($3{\cdot}n_T{\cdot}n_P$).

The axis inversion, compared with Fig. 1, avoids the requirement of quadratic root finding that would be necessary in fits of *sound velocity vs. concentration*. Indeed, where higher order fits are required no analytic solutions might exist. Sound velocity is the measurement variable and the natural choice of abscissa. Axis reversal also implies a redefinition of Eq. (5) as:

$$\partial(mix) = (\partial c * m') \tag{7}$$

where m' is the slope of the *concentration vs. sound velocity* curve. For an example from Fig. 7, at a measured sound velocity of 122.75 ms^{-1}, corresponding to around 10% air contamination the local curve slope (at 20 °C) obtained by differentiating its polynomial form is around 1.73% air/ms^{-1}: a sound velocity measurement error of ± 0.025 ms^{-1} would yield an uncertainty in air concentration of ± 0.04%.

3.2. *Real-time monitoring coolant leaks*

Three further instruments illustrated in Fig. 2 monitor coolant leaks from the ATLAS SCT, Pixel and IBL (Insertable B-Layer) silicon tracker subsystems, which are presently cooled by evaporation of C_3F_8 (SCT & Pixel) and CO_2 (IBL). Gas is aspirated from their separate N_2-purged anti-humidity envelopes into three sonar tubes. The intrinsic sound velocity measurement uncertainty of ± 0.025 ms^{-1} results in respective precisions better than ± 2.10^{-5} and ± 10^{-4}.

The dynamic (alarm) ranges of interest for C_3F_8 and CO_2 coolant leak concentrations into N_2 lie in the molar interval 0–0.1%. Over this relatively short range linear (2-parameter) fits based on 100 sound velocity – concentration points (for example in Fig. 1: generated in 10^{-5} increments) have been found sufficiently precise.

These parameters are generated at points in a temperature-pressure

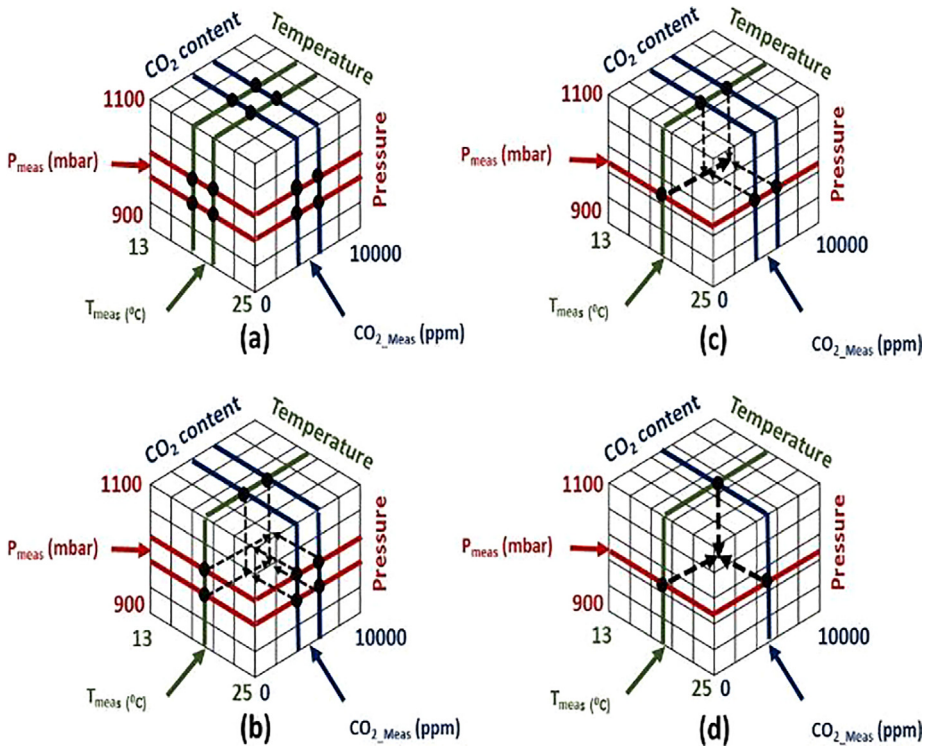

Fig. 8. Schematic showing the sequence of successive interpolation of *sound velocity vs. C_3F_8 concentration fit parameters* from nearest stored grid values to determine the fit parameters corresponding to the measured pressure, temperature and CO_2 contamination (see text).

grid from 13 to 25 °C (step 0.5 °C: $n_T = 25$ points) and 900–1100 $mbar_{abs}$ (step 20 mbar: $n_P = 11$ points) using NIST-REFPROP [4]. In the case of the IBL sub-detector this results in a database of 550 stored parameters ($2 \cdot n_T \cdot n_P$).

In the case of the Pixel and (particularly) the SCT sub-detectors the N_2 envelopes can become contaminated with CO_2 from adjacent systems. Parameters for fits to *C_3F_8 concentration vs. sound velocity* are therefore generated points on a 3-D *temperature-pressure-CO_2* grid from 13 to 25 °C (step 0.5 °C: $n_T = 25$ points) and 900–1100 $mbar_{abs}$ (step 20 mbar: $n_P = 11$ points) and 0-10′000 ppm (step 1000 ppm: $n_{CO2} = 11$ points) using [4], resulting in a database of 6050 stored parameters ($2 \cdot n_T \cdot n_P \cdot n_{CO2}$). In these circuits CO_2 concentration is measured with Telaire® infra-red sensors [8] with 10′000 ppm full scale output.

In practice the temperature, pressure and CO_2 concentration (measured simultaneously with acoustic transit times) will fall between the grid values: a multi-step interpolation is followed, as illustrated in Fig. 8:

- *sound velocity – C_3F_8 concentration* fit para-meters are first identified from the database at the eight nearest grid points in (*Pressure, Temperature, CO_2 ppm*) space defining the smallest cuboidal volume encompassing the process measurable P_{meas}, T_{meas} and CO_{2_meas}. For clarity these eight core grid points are represented by their projections on the (*Pressure, Temperature*), (*Pressure, CO_2 ppm*) and (*CO_2 ppm, Temperature*) facets, as shown in Fig. 8(a):
- *sound velocity – C_3F_8 concentration* fit para-meters are then interpolated to intermediate values corresponding to T_{meas} at grid pressures immediately above and below P_{meas}, as illustrated in Fig. 8(b), collapsing the search at the core of the grid to a 2-D search between 4 grid points in (*Pressure, CO_2 ppm*) space;
- an interpolation between these intermediate *sound velocity – C_3F_8 concentration* fit para-meters is then made along the orthogonal (pressure) direction to calculate the parameters corresponding to T_{meas}, as illustrated in Fig. 8(c), further collapsing the core search to a final interpolation between 2 adjacent grid points the *CO_2 ppm* direction:
- an interpolation between these intermediate *sound velocities vs. C_3F_8 concentration* fit parameters is then made along the *CO_2 ppm* direction to calculate the final parameters corresponding to P_{meas}, T_{meas}, and CO_{2_meas}, as illustrated in Fig. 8(d). From these parameters the relative concentrations of the C_3F_8 and N_2 components in the mixture of interest are calculated. In the case where no third-party gas can contribute to the primary mixture, the interpolation reduces to a 2-D search between 4 grid points in (*Temperature*, *Pressure*) space as in the case of the IBL system.

3.2.1. Measurements in the pixel sub-system

Fig. 9 illustrates the change in effective C_3F_8 concentration in the N_2-purged envelope surrounding the ATLAS Pixel subsystem following simultaneous start-up of its 88 C_3F_8 evaporative cooling sub-circuits in January 2018. A similar increase in C_3F_8 concentration was seen in the envelope cooling start-ups in 2016 and 2017 [2], rising from <

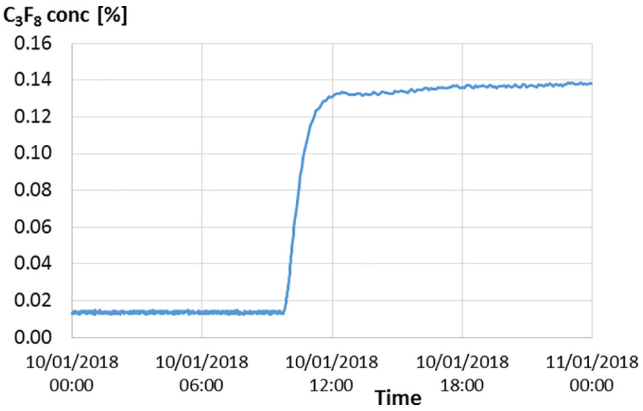

Fig. 9. C_3F_8 concentration from the N_2-purged volume of the ATLAS Pixel detector before and following cooling system turn-on: Jan. 2017 & Jan. 2018.

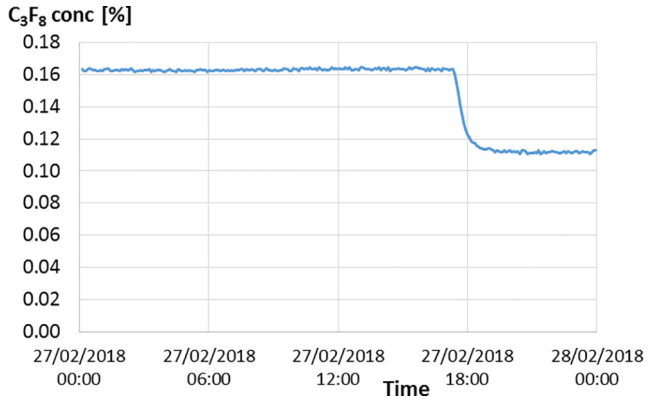

Fig. 10. Change in C_3F_8 concentration in the Pixel detector envelope following a reduction of operating temperature from −5 °C to −20 °C on February 27, 2018.

5.10^{-3}% to around 0.13%, with sensitivity to molar concentration changes better than 2.10^{-3}%. These comparison of leak rates after cooling start-ups indicated that no new leaks had developed in around two years' running of the detector. The coolant leak rate from four identified sub-circuits is presently considered acceptable.

Fig. 10 illustrates the reduction in C_3F_8 concentration preceding and following a reduction of the Pixel detector operating temperature from −5 °C to −20 °C on February 27, 2018.

This reduction in temperature is due to a reduction in the set-point of the evaporation pressure from 3.51 to 2.04 bar_{abs}. The corresponding leak rate from known leaking circuits was consequently reduced.

3.2.2. *Measurements in the SCT sub-system*

The anti-humidity envelope surrounding the much larger SCT sub-detector is divided into four zones from which gas is sequentially monitored in a 16-h supercycle by aspiration through a single sonar instrument. Sample extraction points are chosen to maximize sensitivity to expected localized hydrostatic pooling of heavy C_3F_8 vapor.

Fig. 11 illustrates the variation of C_3F_8 and CO_2 concentration in gas aspirated from the four zones of the ATLAS SCT N_2 anti-humidity envelope during a recent period in February-March 2018.

Importantly, here the relative concentrations of a primary gas pair of interest (C_3F_8 /N_2) are demonstrably measured in 4 different streams of mixture containing known concentrations of a third-party gas, using a data base including that gas, constructed using the formalism of Eqs. (1)–(4).

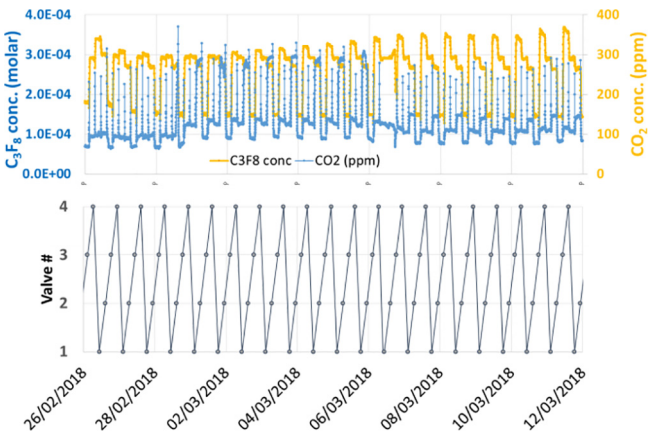

Fig. 11. Variation of the C_3F_8 and CO_2 concentration in gas aspirated from the surrounding the four zones of N_2 anti-humidity envelope of the ATLAS SCT sub-detector over a recent period, February-March 2018.

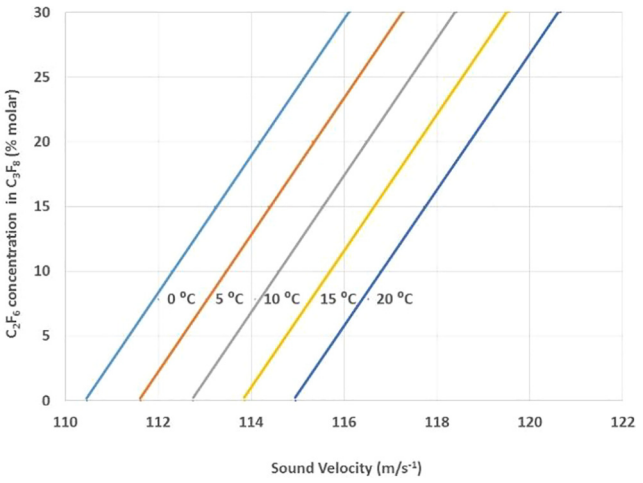

Fig. 12. Variation of sound velocity with molar % C_2F_6 concentration in C_3F_8 over the range 0–30% at several temperatures of the superheated zeotropic blend: pressure 0.1 MPa.

4. Measurements of heat transfer coefficient in C_2F_6/C_3F_8 blends

The evaporative coolants currently used in the ATLAS silicon tracker sub-detectors are radiation-resistant, non-flammable and dielectric, as required in the extreme working environment. The semiconductor materials in the tracker are subject to radiation damage effects which can be mitigated by reducing the operating temperature. Since the sub-detectors and their supply tubing are mostly in inaccessible areas we have investigated the use of a "drop–in" replacement blend for the current C_3F_8 containing up to 25% C_2F_6. Previous studies in representative thermal models of the silicon tracker [9] showed that a temperature reduction of 9 °C from the present −20 °C would be possible using a zeotropic blend containing 25% C_2F_6.(R116). More recently, measurements of the heat transfer coefficient (HTC) in C_2F_6/C_3F_8 blends have been made [10] in 5% steps from 0% to 25% C_2F_6. These blends were prepared by mass mixing and verified in the superheated vapor phase by speed of sound measurements. Fig. 12 illustrates the variation of sound velocity with % molar C_2F_6 concentration in C_3F_8 over the range of interest 0–30%. For example, in a blend with 20% C_2F_6 where the slope of the *concentration vs. sound velocity* curve is $\sim 5.25\%[C_2F_6]^{-1}.ms^{-1}$ the intrinsic sound velocity uncertainty of ± 0.025 ms^{-1} yields via Eq. (7) a concentration uncertainty ± 0.16%.

For measurements of HTC all physical parameters, tube cross section, flow rate and input power were chosen to correspond to those within the ATLAS tracker. The blend density is calculated from component densities, calculated at the measured temperature and pressure [4], then weighted according to the blend ratio determined ultrasonically. The measurements were made in an electrically-heated 4 mm ID copper-nickel tube with 70 µm wall tube at heat fluxes from 3.5 to 10 $kW.m^{-2}$, mass fluxes from 91 to 264 $kg.m^{-2}.s^{-1}$ and vapor quality from 0.35 to a superheated state (dry-out condition) at evaporation pressures from 0.142 to 0.205 MPa. These tests demonstrated that the temperature reduction of 9 °C with 25% C_2F_6 was furthermore achievable at modest values of HTC values ($\sim 3500\ W.m^{-2}.K^{-1}$). Fig. 13 illustrates typical data.

Our HTC measurements were compared with the predictions of several models of flow boiling heat transfer [11] and with the Kattan-Thome-Favrat flow regime map. The results were in average agreement to around 10% with the Shah, Liu-Winterton (L-W) and Kandlikar models; best agreement (within 5%) being seen with the L-W model incorporating a suppression factor for boiling zeotropic mixtures.

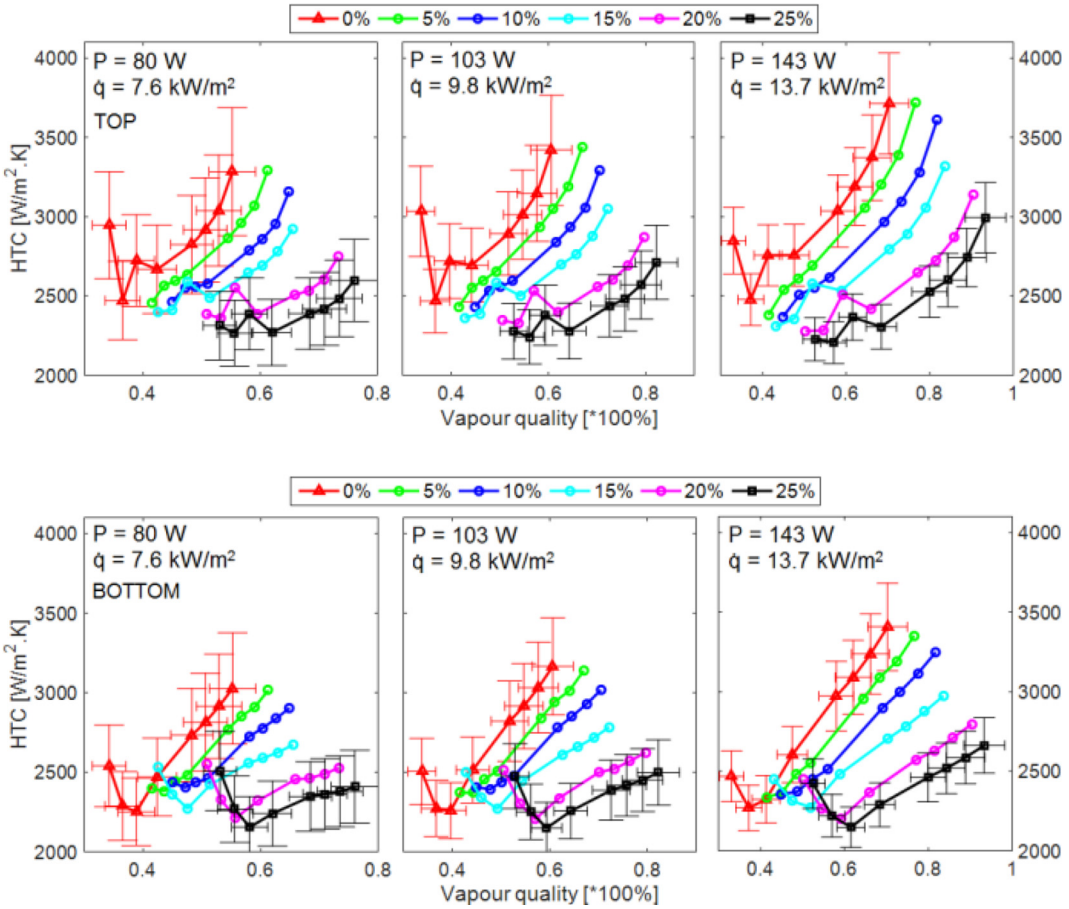

Fig. 13. HTC measured at top (upper row) and bottom (lower row) of a representative tube in various C_2F_6/C_3F_8 blends *vs.* vapor quality and heat flux [10].

5. Conclusion and prospects

We describe several implementations of custom ultrasonic instrumentation for real-time monitoring of flow and binary gas mixtures. One instrument configured as an angled flowmeter demonstrated a precision better than ± 2.3% full scale for air flows up to 10.5 $m.s^{-1}$ and a resolution better than ± 0.05 $kg.s^{-1}$ in C_3F_8 flows around 1 $kg.s^{-1}$. Other instruments have demonstrated a precision in composition measurement of ± 2.10^{-5} in N_2/C_3F_8 and ± 0.16% in C_2F_6/C_3F_8 blends, allowing the creation and monitoring of C_2F_6/C_3F_8 zeotropic blends with well-defined mixing ratios for HTC measurements. Our HTC measurements were compared to several well-known empirical correlations, showing good agreement.

This instrumentation is expected to find use in various industrial and medical applications were accurate and simultaneous real-time flow and gas analysis are required. The ultrasonic instrument is based on commercial transducers controlled by an electronic system. This device can be therefore assembled quite easily and this represent one of the force point for the diffusion of this tool in different application. As an example it can be used to precisely monitor the concentration balance of the anesthetic gas mixtures during the surgical operation Although ultrasonic gas analysis is primarily a binary gas analysis tool, we have demonstrated that it can be successfully used with higher order gas mixtures if the concentration of the additional component is known from another source and the reference database includes the third-party gas.

The combination of ultrasonic binary gas analysis with other measurement technologies allowing a multi-gas analysis capability is useful in many applications: - for example in clinical anesthesia where gas mixtures contain more than two components. Similarities can be drawn between our studies in C_3F_8/N_2 (m.w. 188/28) with third party CO_2 (m.w. 44) and the mixtures of similar molecular weight difference encountered in the developing area of xenon-based anesthesia (Xe/O_2: m.w. 131/29).

Preliminary ultrasonic studies in Xe/O_2 blends were recently reported [12]. Fig. 14 illustrates the *composition/sound velocity* dependence at atmospheric pressure for several temperatures.

The steep dependence (average around 0.52% per $m.s^{-1}$ over the clinical range from 20 to 100% O_2) typically requires a 5th order polynomial representation, with mixture precision depending on the sound velocity measurement uncertainty according to eq. (7).

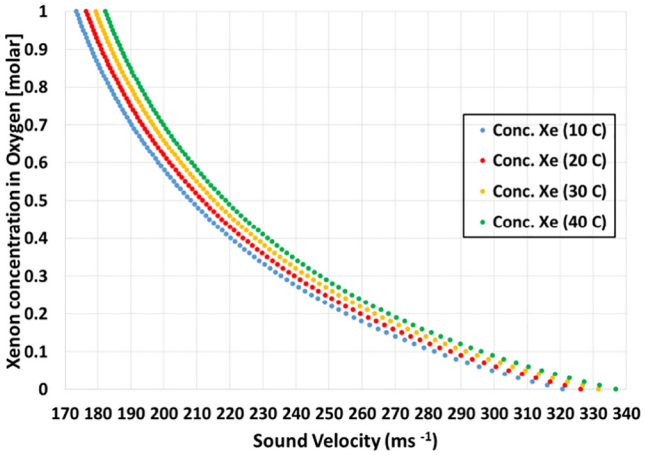

Fig. 14. *Composition/sound velocity* dependence in xenon–oxygen mixtures at atmospheric pressure and several temperatures.

A target precision of ± 0.1% Xe implies a sound velocity measurement precision of ± 0.19 $m.s^{-1}$. While precisions of 0.025–0.05 ms^{-1} are achieved in the CERN instruments using exposed foil capacitative transducers [1], such precision is more challenging over shorter acoustic paths using piezoelectric transducers mounted in sterilisable enclosures having reduced acoustic coupling to gases. New custom ultrasonic instrumentation is currently under development to improve the precision of xenon delivery during anaesthesia [12] and to reduce wastage in the post-operative environment by allowing xenon to be extracted from recovered breathing gas mixtures for recycling.

Acknowledgements

This research was carried out through the participation of the authors in the CERN ATLAS collaboration. M. Doubek and V. Vacek acknowledge also support from the Department of Physics of the Faculty of Mechanical Engineering at the Czech Technical University in Prague and through grant MSMT No.:1501601D000 LM2015058

References

[1] Originally by Polaroid® for autofocus cameras: now marketed as the SensComp model 600 transducer, http://www.senscomp.com/ultrasonic-sensors/.
[2] R. Bates, et al., A combined ultrasonic flowmeter and binary vapour mixture analyzer for the ATLAS silicon tracker, J. Instrum. JINST 8 (2013) P02006.
[3] G. Hallewell et al., The use of a 90 metre thermo-siphon cooling plant and associated custom ultrasonic instrumentation in the cooling of the ATLAS inner detector, in: Proc. 16th Intl. Conf. on Accelerator and Large Experimental Physics Control Systems (ICALEPCS2017): Barcelona, Oct 8–13 2017. http://accelconf.web.cern.ch/AccelConf/icalepcs2017/papers/thpha193.pdf.
[4] E. Lemmon, M. Huber, M. McLinden, 'REFPROP' Standard reference database 23, version 9.0, U.S, National Institute of Standards and Technology, 2010.
[5] M. Battistin, et al., Novel ultrasonic instrumentation developments for real-time monitoring of binary gas mixtures and flow: description and applications, Sens. Transducers 207 (12) (2016) 4–14.
[6] M. Battistin, et al., The thermosiphon cooling system of the ATLAS experiment at the CERN Large Hadron Collider, IJCRE (2015) 13511–13521.
[7] R. Bates, et al., A custom online ultrasonic gas mixture analyzer with simultaneous flowmetry, developed for the upgraded evaporative cooling system of the ATLAS silicon tracker, IEEE Trans. Nucl. Sci. 61 (4) (2014) 2059–2065.
[8] Amphenol Telaire infrared CO2 monitor: https://www.amphenol-sensors.com/en/products/telaire-air-quality.
[9] R. Bates, et al., The cooling capabilities of C_2F_6/C_3F_8 saturated fluorocarbon blends for the ATLAS silicon tracker, J. Instrum. 10 (03) (2015) P03027.
[10] M. Doubek, et al., Measurement of heat transfer coefficient in two phase flows of radiation-resistant zeotropic C_2F_6/C_3F_8 blends, Int. J. Heat Mass Transfer 113 (2017) 246–256.
[11] M. Doubek et al., Experimental investigation and modelling of flow boiling heat transfer of C2F6/C3F8 blends, in: Proc. 13th Intl. conf. on Heat transfer, Fluid Mechanics and Thermodynamics (HEFAT2017), Portoroz, Slovenia 17–19 July 2017. https://repository.up.ac.za/handle/2263/62434.
[12] D. Williams, G. Hallewell, E. Chakkarapani, J. Dingley, Real-time measurement of Xenon in a binary gas mixture using ultrasound time-of-flight: a feasibility study, in: Proc. Euroanaesthesia 2017, Geneva, June 3–5, 2017. http://euroanaesthesia2017.esahq.org/ Anesth Analg. 2018 Oct 3. doi:10.1213/ANE.0000000000003806. [E-pub ahead of print] PMID: 30286009.